Control of defect structure in compound semiconductors with stoichiometry: Oxygen in CdTe

G. Chen, I. Miotkowski, S. Rodriguez, and A. K. Ramdas
Department of Physics, Purdue University, West Lafayette, Indiana 47907, USA
(Received 21 November 2006; revised manuscript received 10 January 2007; published 14 March 2007)

Two types of localized vibrational modes of oxygen substituting for Te in CdTe, i.e., O_{Te}, are reported. In one, O_{Te} is associated with a nearest neighbor (NN) vacancy as a (O_{Te}-V_{Cd}) center and hence with C_{3v} symmetry, with its uniaxial axis along ⟨111⟩, whereas in the other, O_{Te} is surrounded by all the four NN Cd's and thus possesses T_d site symmetry. By an appropriate control of stoichiometry it is possible to reproducibly generate the formation of either (O_{Te}-V_{Cd}) or O_{Te} centers. These configurations are deduced from their ultrahigh resolution infrared signatures. For the (O_{Te}-V_{Cd}) centers, consistent with their uniaxial symmetry, a pair of sharp local vibrational modes (LVM) are observed at $\nu_1=1096.78$ cm^{-1} and $\nu_2=1108.35$ cm^{-1}, the latter nearly twice as intense as the former. In the LVM spectrum of O_{Te} centers with the full complement of NN Cd's, consistent with its T_d symmetry, only one LVM signature appears at $\nu_0=349.79$ cm^{-1}. With the increasing temperature, ν_1 and ν_2 approach each other and coalesce into a single triply degenerate line at ν_0^* for temperature $T \geq T^* \sim 300$ K; the uniaxial (C_{3v}) symmetry of (O_{Te}-V_{Cd}) transforms to T_d symmetry at T^* and above, acquired by the (O_{Te}-V_{Cd}) centers due to the increasing rate of bond switching among the four possible O_{Te}-V_{Cd} ⟨111⟩ directions as T approaches T^*. The (O_{Te}-V_{Cd}) centers also display a fascinating pair of second harmonics including a coalescence at T^* and beyond.

DOI: 10.1103/PhysRevB.75.125204 PACS number(s): 61.72.Ji, 63.20.Pw, 78.30.Fs

I. INTRODUCTION

Among the tetrahedrally coordinated binary semiconductors, the $A^{II}B^{VI}$'s are unique in the large number of elements which can replace the cations as isoelectronic impurities, and, when concentrations are large, result in ternary alloys. Group IIA, group IIB, the 3d transition-metal ions (TMIs), and group VIA elements can all be incorporated in a $A^{II}B^{VI}$ to form the ternary $A^{II}_{1-x}M^{II}_xB^{VI}$ ($M^{II}\equiv$ group IIA, IIB, or 3*d*-TMI) or $A^{II}M^{VI}_xB^{VI}_{1-x}$ ($M^{VI}\equiv$ group VIA). The maximum value of x allowed is determined by crystal chemistry. $Cd_{1-x}Zn_xTe$, $Zn_{1-x}Mn_xTe$, and $CdSe_xTe_{1-x}$ are just a few examples.

The lattice dynamics of II-VI based alloys can be well described by the random element isodisplacement model (REI model) and its modifications.[1,2] The relative masses of the atoms constituting the alloy and the force constants characterizing the interatomic bonds determine the pattern of the evolution of "multimode behavior" of the zone-center optical phonon frequencies as a function of composition.[3] The collective vibrations involving the zone-center phonons at high concentration of M^{II} (M^{VI}) emerge from the localized vibration of the M^{II} (M^{VI}) when present in extreme dilution. Such an evolution of the local mode of substitutional Mg^{2+} in CdTe into collective zone-center "MgTe-like" LO and TO modes has been reported by Oh *et al.*,[4] for example. In this context, it is of fundamental interest to study the localized vibrations as a starting point towards an understanding of the vibrational properties of the multinary semiconductor alloys.

Localized vibrational modes (LVM) occur when the defect consists of an impurity atom lighter than the atoms of the host crystal, provided the force constants between this atom and its neighbors have the strengths similar to those between pairs of the host crystal atoms. In II-VI semiconductors, all the 3*d*-TMIs and part of group IIA and VIA atoms are lighter than the cations (Zn, Cd, or Hg) as well as the anions (Se or Te). Thus the replacement of the cation or anion by these lighter atoms leads to an LVM frequency above that of the reststrahlen. Mayur *et al.*[5] have studied 3*d*-TMI LVMs in the II-VI semiconductors in great detail, and the group IIA and VIA impurity LVMs were extensively investigated by Sciacca *et al.*[6,7] While the LVMs of S in CdTe were discovered by Sciacca *et al.*,[6] the LVM of oxygen in CdTe has been elusive until recently. A brief report on oxygen LVMs in CdTe has been published recently.[8]

In this paper, we present a detailed study on the LVM spectra of the two types of oxygen centers in CdTe on the basis of their infrared signatures recorded with an ultrahigh resolution Fourier transform spectrometer. By adopting specific crystal growth strategies, Cd vacancies (V_{Cd}) are either generated or suppressed deliberately. In the former, oxygen is bonded to three Cd nearest neighbors (NN) and occurs near a Cd vacancy, where the fourth Cd would have been; we refer to this complex as "O_{Te}-V_{Cd}" with C_{3v} symmetry. In the latter, oxygen is incorporated with full complement of all four NN Cd's to which the O_{Te} with T_d symmetry is tetrahedrally bonded. The two oxygen centers display unique infrared signatures which bear unmistakable imprints of their site symmetry.

II. EXPERIMENTAL

A. Crystal growth

Single crystals of CdTe were grown by the vertical Bridgman technique using a two-zone furnace with a linear temperature gradient of 5 °C/cm in the growth zone.[9] All the starting materials used for crystal growth were deoxidized and purified further by multiple vacuum distillation. The raw material was synthesized from pure CdTe and appropriate amounts of TeO_2 or CdO. The synthesis was made in carbon-covered ampoules to avoid potential reaction with the quartz wall of the ampoules. After the synthesis was complete, the prereacted charge was carefully outgassed at temperatures below 500 °C under dynamic vacuum to remove any unreacted components. The pre-reacted material was placed in a

quartz ampoule of 12–15 mm internal diameter which was covered from inside with multiple layers of carbon by pyrolysis of spectrographic purity acetone. The growth ampoule was then placed in a quartz holder, which could easily be inserted into the alumina-tube liner by a lift-up mechanism. The radial gradient inside the growth zone was symmetric and estimated to be less than 0.5 °C/cm. The typical speed for moving the CdTe:O ampoule through the temperature gradient was between 1.2 and 1.8 mm/h.

B. Experimental techniques

The absorption spectra were recorded using an ultrahigh resolution BOMEM DA.3 Fourier transform infrared (FTIR) spectrometer[10] capable of an ultimate unapodized resolution of 0.0026 cm^{-1}. A composite Si liquid helium bolometer for the 10–700 cm^{-1} range, a HgCdTe-infrared detector for the 500–5000 cm^{-1} range, and an InSb detector for the 1800–8500 cm^{-1} range were employed. A Janis 10DT Supervaritemp[11] optical cryostat, with polypropylene windows along one axis and wedged ZnSe inner and CsI outer windows along the other axis, allowed measurements in the range of 1.8–300 K. The incident light is unpolarized due to the special features in the optical layout of the interferometer. The specimens were prepared for infrared absorption measurements by suitably polishing two approximately plane parallel surfaces, with a small wedge introduced to avoid channelling in the spectrum.

III. EXPERIMENTAL RESULTS AND DISCUSSION

A. (O_{Te}-V_{Cd}) centers in CdTe

1. Fundamental transitions

During the search for an oxygen LVM in CdTe, we persistently observed a pair of very sharp lines with remarkably small full widths at half maximum (FWHM) (see Fig. 1). Oxygen was introduced during the crystal growth by the addition of CdO to the starting material, the concentration of the nonstoichiometry-related Cd vacancies remaining close to that in pure CdTe.[12] The two extremely sharp infrared signatures $\nu_1 = 1096.78$ cm^{-1} and $\nu_2 = 1108.35$ cm^{-1} in the figure, recorded with the FTIR spectrometer set to 0.01 cm^{-1} resolution, have FWHMs of 0.165 and 0.137 cm^{-1}, respectively; in addition, the intensity of ν_2 is nearly twice that of ν_1.

In view of the doublet character of the LVMs, we consider the signatures to arise from a defect with C_{3v} (uniaxial) symmetry. Postulating that oxygen replaces an isovalent Te anion in the vicinity of a Cd vacancy (see the model shown in Fig. 2), the defect center O_{Te}-V_{Cd} along with the three Cd's bonded to O_{Te} displays the local symmetry C_{3v}. Cd vacancies are known to arise in CdTe during growth as a consequence of nonstoichiometry. In order to prove that the center indeed involves oxygen in this manner, we made two series of samples doped with different concentrations of oxygen, while simultaneously increasing V_{Cd} concentration. CdO is added to the starting material to provide oxygen and in order to increase the V_{Cd} concentration, additional Te is added. As shown in Fig. 3, the intensities of the doublet increase as the oxygen concentration increases, confirming our conjecture that the defect consists of Cd vacancy in association with an oxygen replacing Te substitutionally. Another equally successful strategy for the crystal growth of CdTe in which oxygen is incorporated with C_{3v} symmetry is one in which TeO_2 is added to the CdTe charge prior to crystal growth. It can be

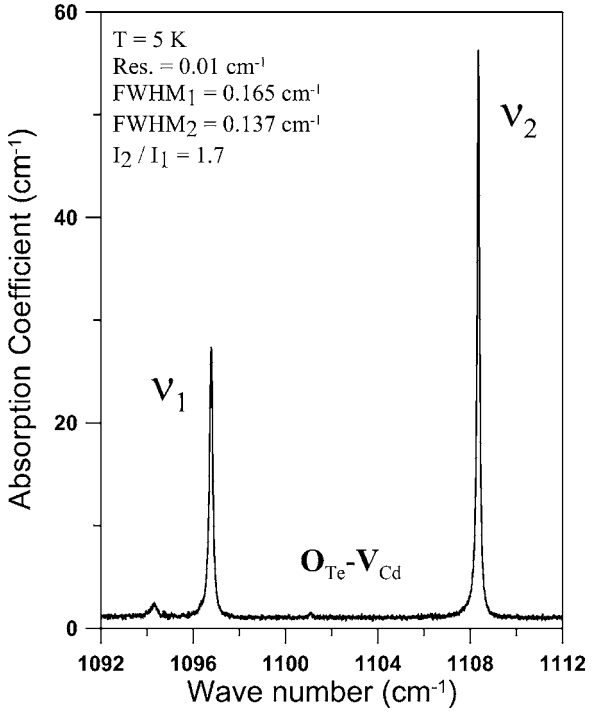

FIG. 1. The infrared absorption spectrum of the "O_{Te}-V_{Cd}" center with C_{3v} symmetry in CdTe:O. Recorded at 5 K with a FTIR spectrometer set at 0.01 cm^{-1} resolution.

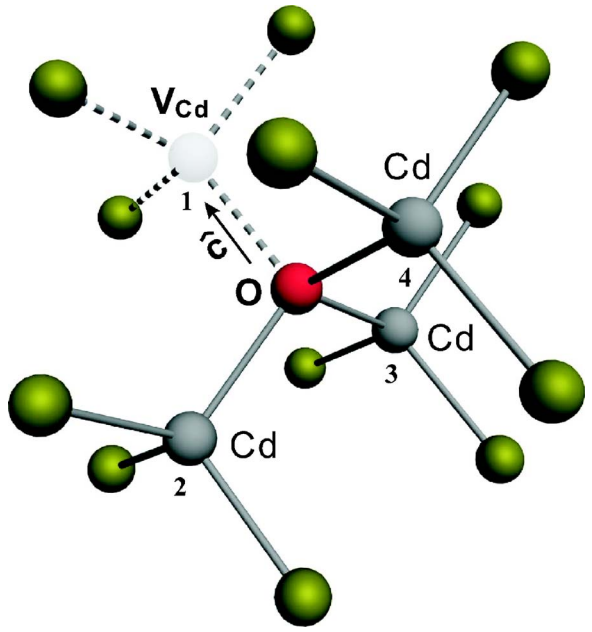

FIG. 2. (Color online) The figure shows a three-dimensional model of substitutional oxygen replacing Te (O_{Te}), its three nearest neighbor Cd atoms, but with a vacancy (V_{Cd}) at the site of the fourth Cd. The unlabeled atoms in the model are the Te atoms.

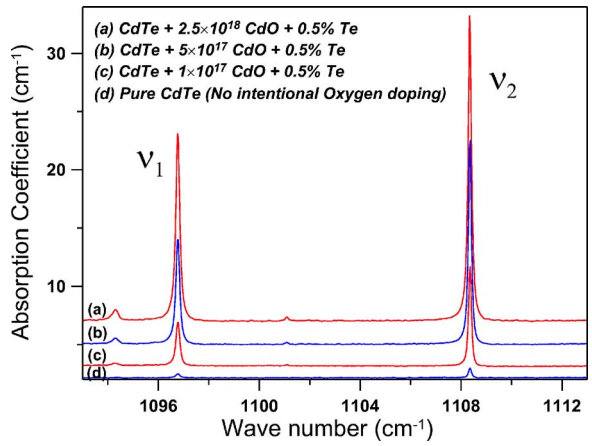

FIG. 3. (Color online) The infrared absorption spectra of CdTe:O with different concentrations of CdO and excess Te recorded at 5 K. The spectra are displaced vertically for clarity.

seen that, for each TeO_2 unit destroyed, two O's and one Te will be released. Te released in this process produces a corresponding additional number of vacancies. The intensities of ν_1 and ν_2 also increase with increasing TeO_2. Thus one can claim that ν_1 and ν_2 are oxygen-related LVMs associated with the O_{Te}-V_{Cd} centers.[13]

Each O_{Te}-V_{Cd} center is characterized by a $\hat{\mathbf{c}}$ axis along [1 1 1], [$\bar{1}$ $\bar{1}$ 1], [$\bar{1}$ 1 $\bar{1}$], or [1 $\bar{1}$ $\bar{1}$]. The two infrared active LVMs of O_{Te}-V_{Cd} (we are for the moment assuming the three NN Cd's in turn bonded to the rest of the crystal do not move) are given by group theory to be Γ_1 and Γ_3 (in the notation of Koster *et al.*[14]); in the nondegenerate Γ_1 mode, oxygen vibrates along $\hat{\mathbf{c}}$ whereas in the doubly degenerate Γ_3, its motion is confined to the plane perpendicular to $\hat{\mathbf{c}}$. The Γ_1 mode responds to light polarized $\parallel \hat{\mathbf{c}}$ whereas the Γ_3 doublet couples to light polarized $\perp \hat{\mathbf{c}}$ [see Fig. 2 and Fig. 4(a)]. We note that the O_{Te}-V_{Cd} centers are distributed throughout the crystal with equal populations in each of the four directions of $\hat{\mathbf{c}}$, displaying thus an "orientational" degeneracy. It can also be shown that the polarization effects are then averaged in such a fashion that no net polarization is expected for ν_1 and ν_2, independent of the direction of propagation; the anisotropy of an individual center remains concealed (latent) in the otherwise cubic symmetry of the host.[15] The level ordering shown for the excited states for the fundamental of ν_1 and ν_2 as Γ_1 and Γ_3, respectively, is motivated by the latter being nearly twice as intense as the former. A stronger justification for the symmetry assignment will emerge from the experimental results and their analysis presented below.

In Fig. 5, the temperature dependence of ν_1 and ν_2 in the range 5–80 K is displayed. We note that ν_2 decreases with increasing temperature as well as broadens, as most LVM frequencies generally do, due to anharmonic coupling with phonons;[16] in striking contrast, ν_1 actually *increases* while increasing in its width similar to ν_2. For the higher temperatures as seen in Fig. 6(a), ν_1 and ν_2 eventually coalesce at $T^* \sim 300$ K, behaving for $T > T^*$ as a single mode of frequency ν_0^*, which decreases as the temperature increases. What has happened is that two modes $[\nu_1(\Gamma_1)$ and $\nu_2(\Gamma_3)]$ of the C_{3v} site symmetry of the $(O_{Te}$-$V_{Cd})$ center finally coalesce at around T^*. We propose that a dynamic switching of

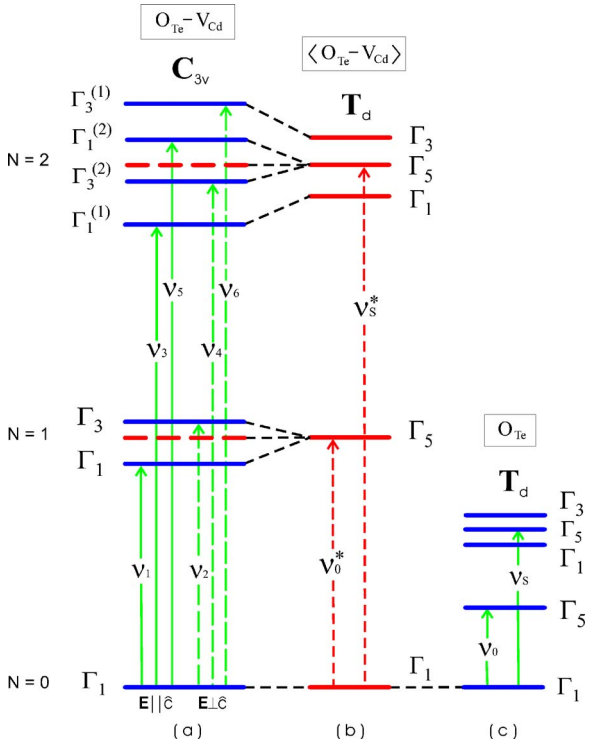

FIG. 4. (Color online) Schematic energy level diagrams and the electric dipole allowed transitions in (a) O_{Te}-V_{Cd} center with C_{3v} site symmetry, (b) O_{Te}-V_{Cd} with the dynamic switching of the dangling bond included, labeled as $\langle O_{Te}$-$V_{Cd}\rangle$, and (c) O_{Te} center with T_d site symmetry.

the O_{Te}-V_{Cd} dangling bond among the four $\langle 111\rangle$ directions for $\hat{\mathbf{c}}$ takes place at an increasing rate; equivalently, one can view V_{Cd}, originally at position 1 in the model shown in Fig. 2, occupying the positions denoted by 1, 2, 3, or 4 with equal probability for $T \geq T^*$ such that the center effectively acquires T_d site symmetry. We denote the center as $\langle O_{Te}$-$V_{Cd}\rangle$ to underscore the O_{Te}-V_{Cd} which has thus experienced a temperature averaged, *acquired* T_d symmetry. Thus we interpret ν_1 and ν_2 to originate from the splitting of ν_0^* as a consequence of Γ_5 of T_d decomposing into Γ_1 and Γ_3 of C_{3v}, the symmetry of $(O_{Te}$-$V_{Cd})$ at the lower temperatures. In the spirit of this splitting, viewed as resulting from a *small* perturbation, $\nu_2(\Gamma_3)$ is expected to be twice as intense as $\nu_1(\Gamma_1)$, the latter shifted twice as much below ν_0^* as $\nu_2(\Gamma_3)$ is above their weighted mean. Continuing this line of argument, one can deduce $\nu_0^* = (\nu_1 + 2\nu_2)/3$ for each temperature as shown in Fig. 6(a). It is particularly impressive that ν_0^* derived in this manner melds so smoothly with that experimentally observed above T^*. As shown in Fig. 6(b), at 330 K ($>T^*$) the single infrared active mode for $\langle O_{Te}$-$V_{Cd}\rangle$ center is observed to occur at $\nu_0^* = 1101.75$ cm^{-1} with FWHM = 15.13 cm^{-1}. Experiments performed with decreasing temperature show a complete restoration of the (ν_1, ν_2) doublet below T^*, demonstrating that (ν_1, ν_2) below and ν_0^* above T^* are completely interconvertible.

The decrease of $(\nu_2 - \nu_1)$, from 11.57 cm^{-1} at 2 K to zero at T^* is remarkable. If one were to assume that the temperature dependence of $(\nu_2 - \nu_1)$ is given by

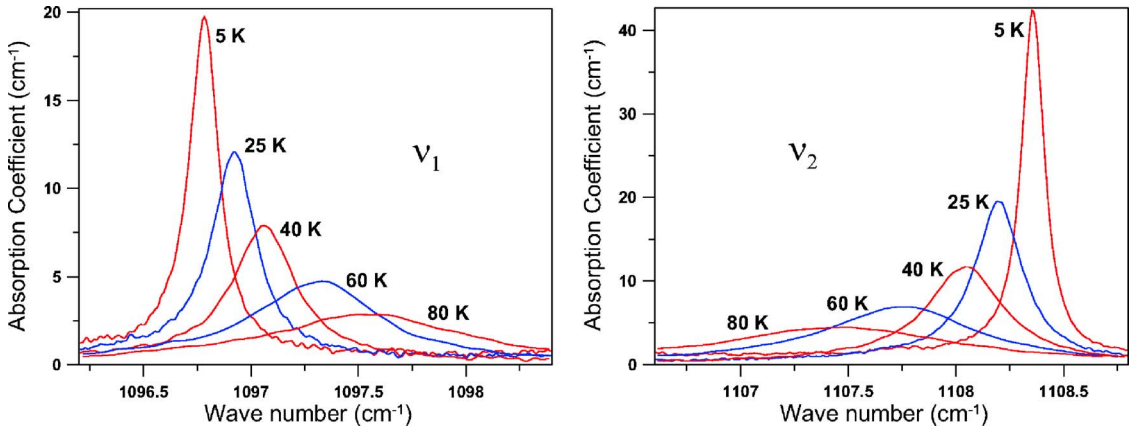

FIG. 5. (Color online) Temperature dependence of ν_1 and ν_2 in the range of 5–80 K. As temperature increases, both ν_1 and ν_2 broaden but ν_2 decreases whereas ν_1 increases.

$$(\nu_2 - \nu_1)_T = (\nu_2 - \nu_1)_0[1 - e^{-W/kT}], \quad (1)$$

$(\nu_2-\nu_1)_T$ and $(\nu_2-\nu_1)_0$ being the separations at T and 0 K, respectively, and W, a single activation energy for the underlying process, the plot of $\ln[1-(\nu_2-\nu_1)_T/(\nu_2-\nu_1)_0]$ vs T^{-1} would yield a straight line. That this is not the case is evident in Fig. 7; rather, one obtains a curve resembling Fig. 3 in Fukai and Sugimoto,[17] presumably associated with the multiple steps necessary for the dangling bond to switch from one $\hat{\mathbf{c}}$ axis to another. While there is no single activation energy in the process, it does yield a straight line at temperatures close to T^*, as one would expect for a typical over-barrier process, yielding $W \sim 42$ meV. It is relevant to note that in their electron paramagnetic resonance experiments on the vacancy trapped next to substitutional P (Si-E center) in electron irradiated, phosphorus doped Si, Watkins and Corbett[18] discovered motional effects at temperatures as low as 250–300 K associated with the destruction and reconstitution of the bonds between Si atoms which are next nearest neighbors. The mechanism for the phosphorus-vacancy reorientation is that the vacancy in the nearest neighbor position with respect to phosphorus makes two jumps away from it and then returns to a new nearest site, the entire process requiring four moves. In the case of the oxygen-vacancy reorientation in CdTe, there are two possible mechanisms which can convert a C_{3v} site symmetric center into an acquired T_d site symmetric one. In the first mechanism the Cd-vacancy shifts positions among the four NN sites of the oxygen. The second possibility is that the oxygen interchanges positions with the other three Te atoms around the Cd vacancy. The latter can be eliminated as it requires more steps and energy to complete the process. As shown in Fig. 2, the nearest neighbors of the Cd vacancy are three Te atoms and the oxygen, thus it is very unlikely for the vacancy to jump into the NN Te site and create a Te vacancy and Te_{Cd}, an antisite defect. Therefore, the only possible mechanism for the oxygen-vacancy reorientation is through the direct jump of Cd vacancy from one to the other three NN Cd sites close to O_{Te}.

As other examples of uniaxial defects with orientational degeneracy acquiring higher symmetry, we cite the extensive studies of Haller and co-workers[19,20] on uniaxial defects in Ge and the work of Muro and Sievers[21] in Si who have invoked "dynamic tunneling" as the microscopic process. The (O_{Te}-V_{Cd}) center in CdTe is a unique example of a trigonal defect with orientational degeneracy in a cubic crystal acquiring the higher T_d symmetry by a dynamic switching of bonds as the underlying microscopic process and revealed in their LVMs through their temperature dependence. The increasing width of ν_1 and ν_2 and the decrease of ν_0^* as a function of temperature follows a behavior pattern not unlike that of the LVM of H^- in CaF_2 by Elliott *et al.*[16] who invoked anharmonic interactions with the host lattice vibra-

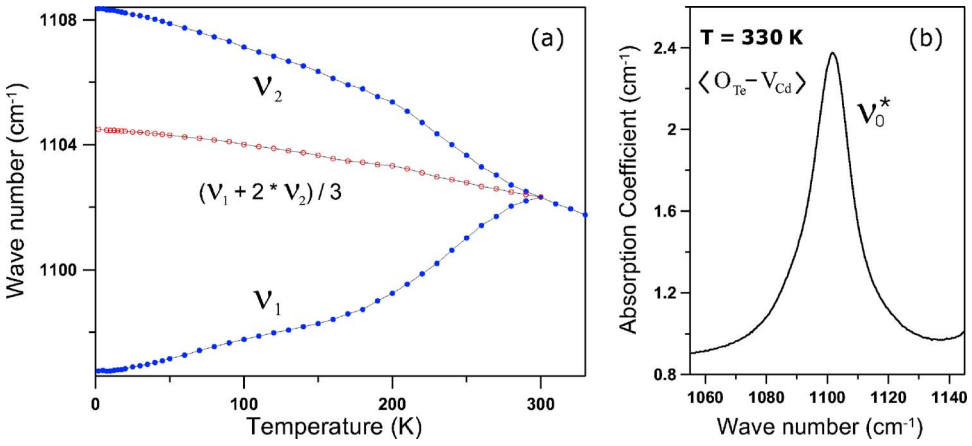

FIG. 6. (Color online) (a) Temperature dependence of ν_1 and ν_2 for the O_{Te}-V_{Cd} center from 2 to 330 K (solid circles) and the weighted average of ν_1 and ν_2, i.e., $\nu_0^*=(\nu_1+2\nu_2)/3$, calculated for each temperature (open circles). (b) The infrared absorption spectrum of the ⟨O_{Te}-V_{Cd}⟩ center with an " acquired" T_d symmetry in CdTe:O recorded at 330 K with a FTIR spectrometer set at 0.5 cm^{-1} resolution.

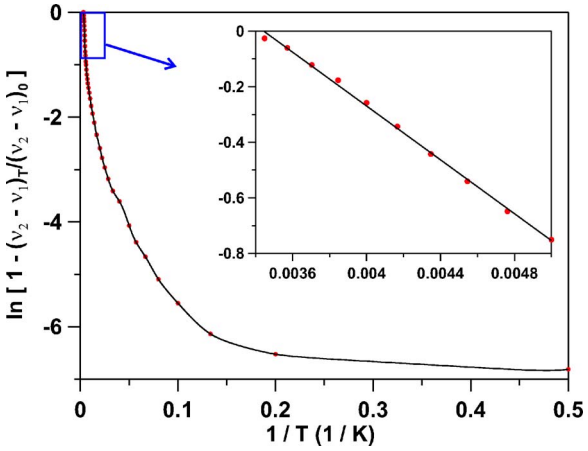

FIG. 7. (Color online) A plot shows $\ln[1-(\nu_2-\nu_1)_T/(\nu_2-\nu_1)_0]$ vs T^{-1} from 2 to 290 K. The inset enlarges the portion of the plot in the range of 200–290 K, and a linear fit is given.

tions to explain the broadening and the shifts.

It is clear from the analysis above that the doublet ν_1 and ν_2 at lower temperature and the single triply degenerate mode ν_0^* at $T \geq T^*$ are related by the dynamic switching of the O_{Te}-V_{Cd} dangling bond. For a small perturbation which deforms the T_d symmetry into C_{3v}, the intensity ratio of ν_2 to ν_1 should be close to 2 (at 5 K, it is 1.65). In Fig. 8, the intensity ratio between ν_2 and ν_1 is plotted as a function of temperature. As temperature increases, the ratio increases from 1.65 to about 2 at ~130 K. This can be understood noting that with increasing temperature, the dynamic switching of the dangling bond becomes more rapid making the O_{Te}-V_{Cd} center closely approach T_d symmetry, and the perturbation correspondingly reduced. This experimental evidence gives a further support for the dynamic switching as the correct interpretation for the coalescence of ν_1 and ν_2 into ν_0^*.

2. Second harmonics

For a three-dimensional harmonic oscillator confined to a T_d site symmetric anharmonic potential, its ground state

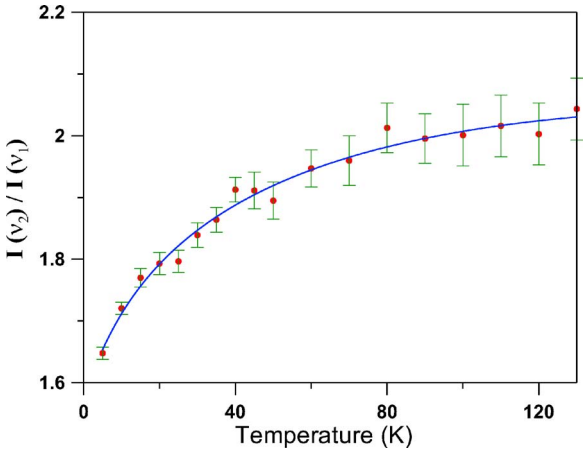

FIG. 8. (Color online) A plot shows the intensity ratio of ν_2 to ν_1 as a function of temperature.

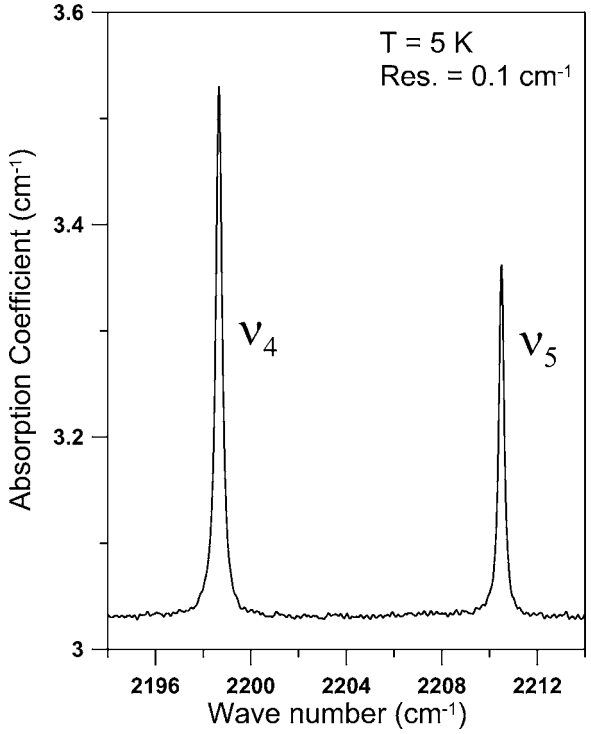

FIG. 9. The absorption spectrum of CdTe:O recorded at 5 K with the FTIR spectrometer set at 0.1 cm^{-1} resolution. The figure shows the second harmonics of local vibrational modes of the (O_{Te}-V_{Cd}) centers.

(with quantum number $N=0$) and the first excited state ($N=1$) levels are of Γ_1 and Γ_5 symmetry, the second harmonic ($N=2$) level splits into three levels given by group theory to be Γ_1, Γ_5, and Γ_3.[14] Among these, the only electric dipole transition from Γ_1 is to the triply degenerate Γ_5 level as shown in Figs. 4(b) and 4(c). When the symmetry of a center degrades from T_d to C_{3v}, the Γ_5 of T_d is further split into two levels with symmetries Γ_1 and Γ_3 of C_{3v}. Thus for a C_{3v} symmetric center the second harmonic state decomposes into four levels labeled as $\Gamma_1^{(1)}$, $\Gamma_3^{(1)}$, $\Gamma_1^{(2)}$, and $\Gamma_3^{(2)}$ in Fig. 4(a). The two transitions from the Γ_1 ground state to the two Γ_1 final states, ν_3 and ν_5, can couple to electric vector $\parallel \hat{\mathbf{c}}$, whereas those to the Γ_3 final states, ν_4 and ν_6, respond to electric vector $\perp \hat{\mathbf{c}}$. We also notice that the transitions to the states $\Gamma_1^{(1)}$ and $\Gamma_3^{(1)}$ will be relatively weak because these states are derived from states which are not infrared active in T_d symmetry.[22] Based on these considerations, we attribute the infrared signatures at 2198.66 and 2210.5 cm^{-1} to ν_4 and ν_5, respectively, as shown in Fig. 9, the choice being made on the basis of ν_4 being stronger than ν_5 by a factor of 2 approximately. It is essential to reemphasize that the C_{3v} symmetry at low temperatures and the T_d symmetry for $T \geq T^*$ for O_{Te}-V_{Cd} centers is connected and interconvertible by the dynamic switching of the dangling bond.

The temperature behavior of the ν_4 and ν_5 lines associated with the (O_{Te}-V_{Cd}) center is shown in Fig. 10. It is striking that ν_5 decreases with increasing temperature, whereas ν_4 does not change much between 5 and 200 K and at temperatures higher than 200 K its frequency increases with temperature; ν_4 and ν_5 also coalesce at $T^* \sim 300$ K, behaving as

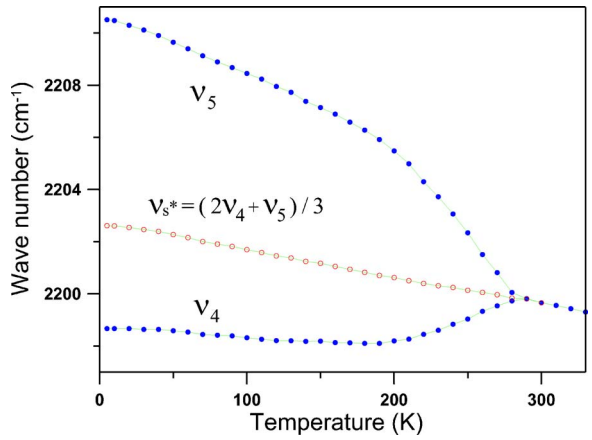

FIG. 10. (Color online) Temperature dependence of ν_4 and ν_5 for the (O_{Te}-V_{Cd}) center from 5 to 330 K (solid circles) and the weighted average of ν_4 and ν_5, i.e., $\nu_s^*=(2\nu_4+\nu_5)/3$, calculated for each temperature (open circles).

a single mode of frequency ν_s^* for higher temperatures, which decreases with increasing temperature. This behavior bears a striking similarity to that of the ν_1, ν_2 pair [Fig. 6(a)]. On the basis of the dynamic switching discussed in that context, we can view ν_4 and ν_5 to originate from the splitting of ν_s^* of Γ_5 in T_d decomposing into Γ_3 and Γ_1 of C_{3v}, the symmetry of (O_{Te}-V_{Cd}) at the lower temperatures. In the same spirit as that applied to ν_1 and ν_2, one can now plot a curve deduced from $\nu_s^*=(2\nu_4+\nu_5)/3$ for each temperature as shown in Fig. 10. Once again, ν_s^* derived in this manner melds with the experimentally observed values above T^*.

As is well known, the localized vibration of a light impurity, of mass M, in a host crystal can be modeled as an oscillator confined to an anharmonic potential consistent with the site symmetry of the impurity. Consider a substitutional impurity and the associated anharmonic potential to possess C_{3v} symmetry. Following Sciacca *et al.*,[6] we use a coordinate system (ξ,η,ζ) in which the ζ axis is parallel to [111], i.e., along the [111] axis of the specific (O_{Te}-V_{Cd}) center under consideration pointing from O_{Te} to V_{Cd}, and ξ and η axes parallel to $[1\bar{1}0]$ and $[11\bar{2}]$, respectively. The fundamental transition in terms of $\omega=2\pi c\nu$, where ω is in rad/s and ν in cm^{-1}, can be shown as

$$\omega_1 = \sqrt{\frac{k_\parallel}{M'}} + \Delta_1 \tag{2}$$

and

$$\omega_2 = \sqrt{\frac{k_\perp}{M'}} + \Delta_2, \tag{3}$$

where $k_\parallel$ and $k_\perp$ are the force constants parallel and perpendicular to the ζ axis ($\hat{\mathbf{c}}$) and M' is the reduced mass and Δ_1 and Δ_2 represent the anharmonic terms defined in the Appendix. The second harmonics are, then,

$$\omega_3 = 2\sqrt{\frac{k_\parallel}{M'}} + \Delta_3, \tag{4}$$

$$\omega_4 = \sqrt{\frac{k_\parallel}{M'}} + \sqrt{\frac{k_\perp}{M'}} + \Delta_4, \tag{5}$$

$$\omega_5 = 2\sqrt{\frac{k_\perp}{M'}} + \Delta_5, \tag{6}$$

$$\omega_6 = 2\sqrt{\frac{k_\perp}{M'}} + \Delta_6, \tag{7}$$

where Δ_3, Δ_4, Δ_5, and Δ_6 represent the anharmonic terms defined in the Appendix .

The contributions coming from the anharmonic terms are small compare to those from the harmonic terms. To the first order approximation, one can show $\nu_4 \approx \nu_1+\nu_2$ and $\nu_5 \approx 2\nu_2$. From these simple relations, the temperature behavior of ν_4 and ν_5 can be explained rather straightforwardly. Figure 6(a) shows ν_1 increases and ν_2 decreases with temperature at about the same rate from 5 to 200 K, thus ν_4 will not change much within this temperature range as been shown in Fig. 10. By comparing Figs. 6(a) and 10, one can see ν_5 decreases about twice as fast as ν_2 which follows from the numerical relationship.

B. O_{Te} centers in CdTe

It is of fundamental interest to enquire if oxygen can be indeed substitutionally incorporated into CdTe with the full complement of the four NN Cd's and hence with T_d symmetry. In order to accomplish this, we grew CdTe crystals with the addition of CdO but with *excess* Cd to provide oxygen on the one hand and to suppress vacancies on the other, and thus create conditions conducive to the formation of centers of oxygen with four Cd's surrounding it. From the knowledge of the LVM of S_{Te} in CdTe,[6] we estimated the spectral range in which to explore the occurrence of the LVM of O_{Te} to be between 325 and 375 cm^{-1}. As can be seen in Fig. 11, we indeed discovered the single infrared active mode of such a center occurring at $\nu_0=349.79$ cm^{-1}. We confirmed this assignment from the unmistakable increase in its intensity with increasing CdO; ν_0 is then the infrared active triply degenerate mode $\Gamma_1 \rightarrow \Gamma_5$ shown in Fig. 4(c). In such specimens, $\nu_1$and ν_2 are absent or occur with extremely low intensities whereas in specimens designed for observing the (ν_1,ν_2) doublet, ν_0 is conspicuous by its absence. The sharp line at 695.72 cm^{-1}, labeled ν_s in Fig. 12, occurs with a frequency very close to $2\nu_0=699.58$ cm^{-1}. We therefore interpret ν_s to be the second harmonic of ν_0 and ascribe the difference to anharmonicity.

C. Comparison of (O_{Te}-V_{Cd}) and O_{Te} centers in CdTe

The weighted average of ν_1 and ν_2, i.e., $(\nu_1+2\nu_2)/3=\nu_0^*$ at 5 K is 1104.49 cm^{-1}, more than three fold higher than ν_0 at 349.79 cm^{-1}. We attribute this to a significant shortening of the Cd-O bonds in the O_{Te}-V_{Cd} centers, followed by the removal of the three fold degeneracy of Γ_5 in T_d, and transforming it into a nondegenerate and a doubly degenerate mode of C_{3v} as reflected in Fig. 4. In order to estimate the

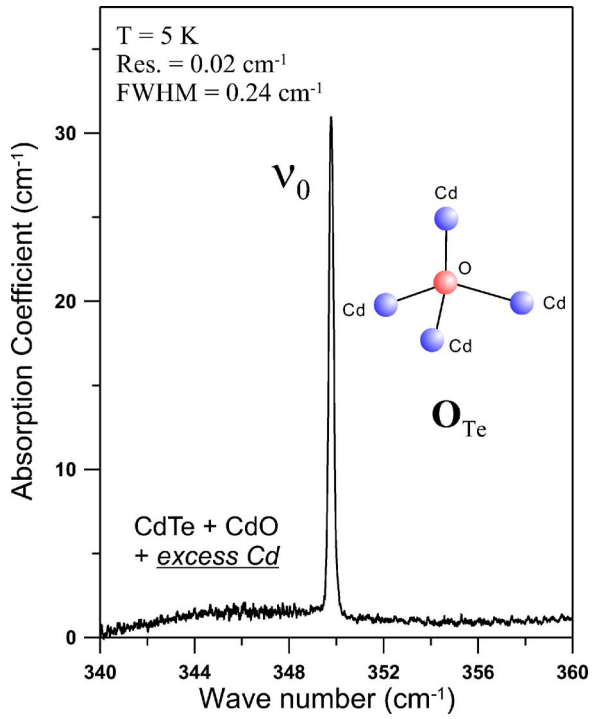

FIG. 11. (Color online) The infrared absorption spectrum of the O_{Te} center with T_d symmetry in CdTe:O recorded at 5 K with a FTIR spectrometer set at 0.02 cm^{-1} resolution. Also shown is the model of O_{Te} along with its four nearest neighbor Cd atoms.

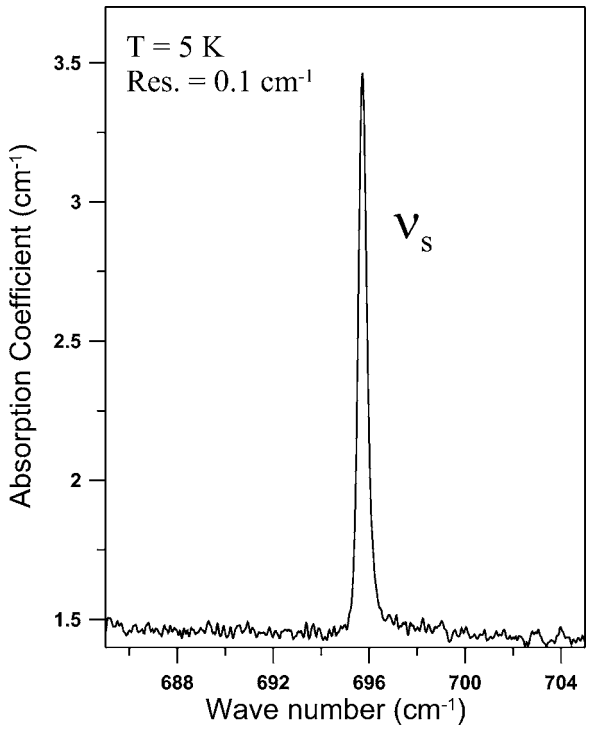

FIG. 12. The infrared absorption spectrum of the O_{Te} center with T_d symmetry in CdTe:O recorded at 5 K with a FTIR spectrometer set at 0.1 cm^{-1} resolution. The single line in the figure is the second harmonic of the LVM of the O_{Te} center.

effect of the decrease in the Cd-O bond length, we carried out a calculation based on the following assumptions. (1) The Cd atoms, bonded to O_{Te} with or without a vacancy in its vicinity, remain fixed due to their significantly larger atomic mass. (2) The interaction between Cd and O is described by a potential associated with changes in bond stretching and bond bending. Although the model shows that ν_1 and ν_2 are larger than ν_0 and $\nu_2 > \nu_1$, the values of the three are comparable. We conclude that perturbation of the Cd-O bond lengths and bond angles in (O_{Te}-V_{Cd}) with respect to those for O_{Te} is too significant to be treated as small to account for ν_1 and ν_2 being ~ threefold larger than ν_0. In this context, we draw attention to the fact that in the (O_{Te}-V_{Cd}) center, the dangling bond pointing from O_{Te} towards the absent Cd cation together with the other three Te-V_{Cd} dangling bonds (model in Fig. 2) define V_{Cd}. In such a vacancy, there will be four electrons associated with the four dangling bonds.[23] It is also worth noting that oxygen is an element with a large electronegativity second only to fluorine.[24] We therefore speculate that the charge cloud associated with V_{Cd} is redistributed into the Cd-O bonds, thereby significantly increasing the effective force constants for ν_1 and ν_2. We qualitatively reflect this in Figs. 4(b) and 4(c), indicative of $\nu_0^* > \nu_0$ by a factor of 3.

The FWHM's of ν_1 and ν_2 of (O_{Te}-V_{Cd}), on the one hand, and ν_0 of O_{Te}, on the other, are displayed in Fig. 13 as a function of temperature. As is evident, ν_1, ν_2 and ν_0 have comparable widths for $T \leq 40$ K but ν_1 and ν_2 are distinctly broader than ν_0 for $T > 40$ K. The reason for this is not far to seek. The melding of ν_1 and ν_2 into ν_0^* at the "coalescence" temperature ~300 K, ascribed to the increasingly rapid

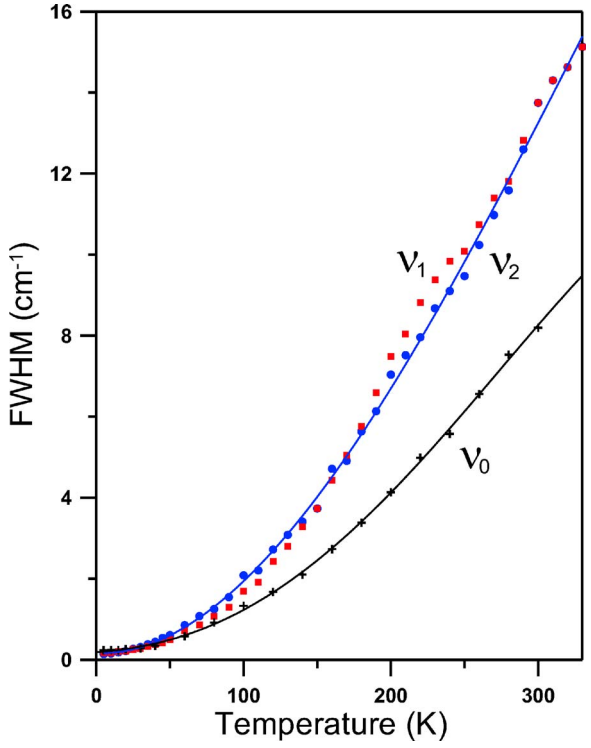

FIG. 13. (Color online) The comparison of the full width at half maximum (FWHM) for ν_1, ν_2, and ν_0 in the region of 5–330 K.

switching of the Cd vacancy occupying positions 1, 2, 3 or 4 with corresponding switch of the dangling bond, would interrupt the normal modes for ν_1 and ν_2. This interruption clearly accounts for their significantly enhanced widths; this process will intensify as T approaches T^*.

IV. CONCLUDING REMARKS

The work reported in this paper demonstrates that the study of local vibrational modes provides unique insights into the environment of a point defect and that it can be deliberately manipulated with stoichiometry. Depending on the site symmetry of the defect center and the associated selection rules, a characteristic pattern of infrared signatures arises. The doublet nature as well as the intensity ratio of the fundamental transitions along with two predominant second harmonic transitions in which their level ordering consistent with the theoretical prediction[22] give unmistakable spectroscopic criteria for ascribing the defect center C_{3v} symmetry; the increase of the doublet intensity with increasing oxygen concentration on the one hand, and the absence of the doublet as a consequence of vacancy suppression on the other, provide strong evidence for the presence of the oxygen in the former and the vacancy in the latter, thus give us solid support to assign the center to be O_{Te}-V_{Cd} with C_{3v} symmetry. The T_d symmetric O_{Te} center is identified on the basis of the corresponding infrared signatures occurring in its fundamental as well as second harmonic regions and the unmistakable increase in absorption with increasing oxygen concentration. The striking temperature behavior of (ν_1, ν_2) as well as (ν_4, ν_5) for $(O_{Te}$-$V_{Cd})$ centers and their coalescence following a simple perturbation theory can be well interpreted on the basis of the dynamic switching of the dangling bond.

Thanks to the low temperature sharpness of their spectroscopic signatures and the essential simplicity of the underlying theoretical considerations, the studies of LVM in semiconductors have led to (a) discovery of well resolved lines according to the isotopic abundance of the impurity, (b) characterization of disorder in a multinary alloy, (c) the host isotopic fine structure,[6,7,25] and in this paper, (d) the unique features associated with perfect stoichiometry and departures therefrom. The present work underscores the important role stoichiometry plays in the impurity configurations in compound semiconductors. On the basis of the simplicity of the two impurity configurations of oxygen in CdTe, achieved reproducibly with controlled growth procedures, it is of interest to enquire if such defects might also occur in many other tetrahedrally coordinated compound semiconductors. In their search, suitable crystal growth strategies and infrared spectroscopy (as in the present case), Raman spectroscopy, and a variety of magnetic resonance techniques can be expected to play a fruitful role.

ACKNOWLEDGMENTS

The authors acknowledge support from the National Science Foundation (Grant No. DMR 0405082) and Purdue University for an Academic Reinvestment grant.

APPENDIX

For convenience, we summarize in this appendix the theoretical background relevant for fundamental and harmonic vibrational modes of defect complexes in terms of site symmetry and anharmonicity. The potential of an anharmonic oscillator of a defect center with T_d site symmetry, referred to the cubic axes (x,y,z) is

$$V(T_d) = \frac{k}{2}(x^2+y^2+z^2) + B(xyz) + D_1(x^4+y^4+z^4) + D_2(y^2z^2+z^2x^2+x^2y^2) + \cdots, \tag{A1}$$

where k is the force constant and B, D_1, and D_2 are the parameters for anharmonic terms. Treating the cubic term to second order and the quartic terms to first order in perturbation theory, the energy levels are given by

$$E_N = \hbar\sqrt{\frac{k}{M'}}\left(N+\frac{3}{2}\right) - \frac{\hbar^2}{24k^2M'}\lambda B^2 + \frac{\hbar^2}{4kM'}(\mu_1 D_1 + \mu_2 D_2), \tag{A2}$$

where $N=0,1,2,\ldots$ and $M'=MM_L/(M+M_L)$ is the reduced mass of the oscillator incorporating a lattice interaction mass M_L to take into account empirically the small motion of the surrounding lattice. The values for μ_1, μ_2, and λ deduced from perturbation theory are given in Table 3 of Newman.[22] As shown in Fig. 4, the electric dipole in T_d transforms as Γ_5 and hence electric dipole transition originating from ground state, which belongs to Γ_1, can only terminate at state having $\Gamma_1 \otimes \Gamma_5 = \Gamma_5$ symmetry. There is one such $\Gamma_1 \rightarrow \Gamma_5$ electric dipole allowed transition in the fundamental and one in the second harmonic. The fundamental transition is given as

$$\omega_0 = \sqrt{\frac{k}{M'}} - \frac{\hbar}{6k^2M'}B^2 + \frac{\hbar}{kM'}(3D_1+D_2) \tag{A3}$$

and the second harmonic transition is

$$\omega_s = 2\sqrt{\frac{k}{M'}} - \frac{\hbar}{2k^2M'}B^2 + \frac{\hbar}{kM'}(6D_1+3D_2). \tag{A4}$$

For a substitutional impurity in a C_{3v} environment, it is advantageous to change from the (x,y,z) coordinates system to (ξ,η,ζ) coordinates in which the ζ axis is parallel to the [111] crystallographic $\hat{\mathbf{c}}$ axis, the ξ and η axes are parallel to $[1\bar{1}0]$ and $[11\bar{2}]$, respectively. In such a coordinate system, the potential can be written as

$$V(C_{3v}) = \frac{k_\parallel}{2}\zeta^2 + \frac{k_\perp}{2}(\xi^2+\eta^2) + B_1\zeta^3 + B_2\zeta(\xi^2+\eta^2) + B_3\left(\xi\eta^2 - \frac{1}{3}\xi^3\right) + C_1\zeta^4 + C_2\zeta^2(\xi^2+\eta^2) + C_3\zeta\xi\left(\eta^2 - \frac{1}{3}\xi^2\right) + C_4(\xi^2+\eta^2)^2, \tag{A5}$$

where $k_\parallel$ and $k_\perp$ are the force constants parallel and perpendicular to the ζ axis ($\hat{\mathbf{c}}$), respectively. The energy levels calculated from perturbation theory are

$$E(N_\xi,N_\eta,N_\zeta) = \hbar\sqrt{\frac{k_\perp}{M'}}(N_\xi+N_\eta+1) + \hbar\sqrt{\frac{k_\parallel}{M'}}(N_\zeta+1/2)$$
$$-\frac{\hbar^2}{8M'}\left(\frac{\alpha B_1^2}{k_\parallel^2}+\frac{\beta B_1 B_2}{k_\parallel^{3/2}k_\perp^{1/2}}+\frac{\gamma B_2^2}{k_\parallel k_\perp}+\frac{\delta B_2^2}{k_\parallel^{1/2}k_\perp(2k_\perp^{1/2}+k_\parallel^{1/2})}+\frac{\epsilon B_2^2}{k_\parallel^{1/2}k_\perp(2k_\perp^{1/2}-k_\parallel^{1/2})}+\frac{\lambda B_3^2}{k_\perp^2}\right)$$
$$+\frac{\hbar^2}{4M'}\left(\frac{\mu_1 C_1}{k_\parallel}+\frac{\mu_2 C_2}{k_\parallel^{1/2}k_\perp^{1/2}}+\frac{\mu_3 C_3}{k_\parallel^{1/4}k_\perp^{3/4}}+\frac{\mu_4 C_4}{k_\perp}\right), \tag{A6}$$

where N_ξ, N_η, $N_\zeta=0,1,2,\ldots$, and M' is again the reduced mass of the oscillator. The values of α, β, …, λ and the μ_i's, the symmetry of states and wave functions, $|N_\xi,N_\eta,N_\zeta\rangle$ are listed in Table I of Sciacca *et al.*[6] The lowering of the site symmetry splits each triply degenerate Γ_5 level of T_d into a single Γ_1 and a doublet Γ_3 of C_{3v} as shown in Fig. 4. The component of the electric dipole along the $\hat{\mathbf{c}}$ transforms as Γ_1 and that perpendicular to $\hat{\mathbf{c}}$ as Γ_3. Therefore, $\Gamma_1\rightarrow\Gamma_1$ is allowed for the electric vector of the incident radiation $\mathbf{E}\|\hat{\mathbf{c}}$, whereas the transition $\Gamma_1\rightarrow\Gamma_3$ is allowed for $\mathbf{E}\perp\hat{\mathbf{c}}$.

The fundamental transitions are given as

$$\omega_1 = \sqrt{\frac{k_\parallel}{M'}}+\Delta_1 \tag{A7}$$

and

$$\omega_2 = \sqrt{\frac{k_\perp}{M'}}+\Delta_2, \tag{A8}$$

and the second harmonic transitions are given as

$$\omega_3 = 2\sqrt{\frac{k_\parallel}{M'}}+\Delta_3, \tag{A9}$$

$$\omega_4 = \sqrt{\frac{k_\parallel}{M'}}+\sqrt{\frac{k_\perp}{M'}}+\Delta_4, \tag{A10}$$

$$\omega_5 = 2\sqrt{\frac{k_\perp}{M'}}+\Delta_5, \tag{A11}$$

and

$$\omega_6 = 2\sqrt{\frac{k_\perp}{M'}}+\Delta_6, \tag{A12}$$

where Δ_1, Δ_2, Δ_3, Δ_4, Δ_5, and Δ_6 are the anharmonic terms expressed as follows:

$$\Delta_n = -\frac{\hbar}{8M'}\left(\frac{\Delta\alpha B_1^2}{k_\parallel^2}+\frac{\Delta\beta B_1 B_2}{k_\parallel^{3/2}k_\perp^{1/2}}+\frac{\Delta\gamma B_2^2}{k_\parallel k_\perp}+\frac{\Delta\delta B_2^2}{k_\parallel^{1/2}k_\perp(2k_\perp^{1/2}+k_\parallel^{1/2})}\right.$$
$$\left.+\frac{\Delta\epsilon B_2^2}{k_\parallel^{1/2}k_\perp(2k_\perp^{1/2}-k_\parallel^{1/2})}+\frac{\Delta\lambda B_3^2}{k_\perp^2}\right)$$
$$+\frac{\hbar}{4M'}\left(\frac{\Delta\mu_1 C_1}{k_\parallel}+\frac{\Delta\mu_2 C_2}{k_\parallel^{1/2}k_\perp^{1/2}}+\frac{\Delta\mu_3 C_3}{k_\parallel^{1/4}k_\perp^{3/4}}+\frac{\Delta\mu_4 C_4}{k_\perp}\right), \tag{A13}$$

where $n=1,2,\ldots,6$, and $\Delta\alpha$, $\Delta\beta$, $\Delta\gamma$, $\Delta\delta$, $\Delta\epsilon$, $\Delta\lambda$, $\Delta\mu_1$, $\Delta\mu_2$, $\Delta\mu_3$, $\Delta\mu_4$ can be calculated from Table I of Sciacca *et al.*[6] by subtracting relevant parameters for the final state from those for the initial state.

[1] Y. S. Chen, W. Shockley, and G. L. Pearson, Phys. Rev. **151**, 648 (1966).
[2] L. Genzel, T. P. Martin, and C. H. Perry, Phys. Status Solidi B **62**, 83 (1974).
[3] A. S. Barker and A. J. Sievers, Rev. Mod. Phys. **47**, S1 (1975).
[4] E. Oh, C. Parks, I. Miotkowski, M. D. Sciacca, A. J. Mayur, and A. K. Ramdas, Phys. Rev. B **48**, 15040 (1993).
[5] A. J. Mayur, M. D. Sciacca, H. Kim, I. Miotkowski, A. K. Ramdas, S. Rodriguez, and G. C. La Rocca, Phys. Rev. B **53**, 12884 (1996).
[6] M. D. Sciacca, A. J. Mayur, N. Shin, I. Miotkowski, A. K. Ramdas, and S. Rodriguez, Phys. Rev. B **51**, 6971 (1995).
[7] M. D. Sciacca, A. J. Mayur, H. Kim, I. Miotkowski, A. K. Ramdas, and S. Rodriguez, Phys. Rev. B **53**, 12878 (1996).
[8] G. Chen, I. Miotkowski, S. Rodriguez, and A. K. Ramdas, Phys. Rev. Lett. **96**, 035508 (2006).
[9] I. Miotkowski, H. Alawadhi, M. J. Seong, S. Tsoi, A. K. Ramdas, and S. Miotkowska, Semicond. Sci. Technol. **20**, 180 (2005).
[10] ABB BOMEM Inc., 585 Charest BLVD East, Suite 300, Québec, Canada, G1K 9H4.
[11] Janis Research Company, Inc., 2 Jewel Drive, Wilmington, MA 01887-0896.
[12] See, for example, P. Rudolph, Prog. Cryst. Growth Charact. Mater. **29**, 275 (1994).
[13] S. A. Awadalla, A. W. Hunt, K. G. Lynn, H. Glass, C. Szeles, and S. H. Wei, Phys. Rev. B **69**, 075210 (2004).
[14] We use the notation for the irreducible representation in G. F. Koster, J. O. Dimmock, R. G. Wheeler, and H. Statz, *Properties of the Thirty-Two Point Groups* (MIT, Cambridge, MA, 1963).
[15] A. A. Kaplyanskii, Opt. Spectrosc. **16**, 329 (1964).
[16] R. J. Elliott, W. Hayes, G. D. Jones, H. F. Macdonald, and C. T. Sennett, Proc. R. Soc. London, Ser. A **289**, 1 (1965).
[17] Y. Fukai and H. Sugimoto, Adv. Phys. **34**, 263 (1985).
[18] G. D. Watkins and J. W. Corbett, Phys. Rev. **134**, A1359 (1964).

[19] E. E. Haller and L. M. Falicov, Phys. Rev. Lett. **41**, 1192 (1978); E. E. Haller, B. Joós, and L. M. Falicov, Phys. Rev. B **21**, 4729 (1980).
[20] B. Joós, E. E. Haller, and L. M. Falicov, Phys. Rev. B **22**, 832 (1980); J. M. Kahn, R. E. McMurray, E. E. Haller, and L. M. Falicov, *ibid.* **36**, 8001 (1987).
[21] K. Muro and A. J. Sievers, Phys. Rev. Lett. **57**, 897 (1986).
[22] R. C. Newman, Adv. Phys. **18**, 545 (1969).
[23] W. Hayes and A. M. Stoneham, *Defects and Defect Processes In Nonmetallic Solids* (John Wiley & Sons, New York, 1984).
[24] L. Pauling, *General Chemistry* (Dover Publications, New York, 1970).
[25] R. C. Newman, Semicond. Sci. Technol. **9**, 1749 (1994): In this comprehensive article the author reviews the literature including many significant contributions on GaAs from his group in which issues relevant to the present paper are addressed.